Robust high-order polarization arrays via vectorial spatial-coherence engineering

Bo Yuan,[1] Zhen Dong,[1] Yonglei Liu,[1,*] Fei Wang,[1,†] Yangjian Cai,[2,3,‡] and Yahong Chen[1,§]

[1] *School of Physical Science and Technology, Soochow University, Suzhou 215006, China*

[2] *Shandong Provincial Engineering and Technical Center of Light Manipulations and Shandong Provincial Key Laboratory of Optics and Photonic Devices, School of Physics and Electronics, Shandong Normal University, Jinan 250014, China*

[3] *Joint Research Center of Light Manipulation Science and Photonic Integrated Chip of East China Normal University and Shandong Normal University, East China Normal University, Shanghai 200241, China*

(Received 18 August 2023; revised 15 October 2023; accepted 2 November 2023; published 15 November 2023)

Beam arrays with structured polarization states offer distinct advantages over single-structured beams in various applications. In this work, we propose an alternative way to synthesize the beam arrays carrying the controllable spatially inhomogeneous polarization states on the higher-order Poincaré spheres. The protocol is based on the vectorial spatial-coherence engineering of a partially coherent beam source, wherein a higher-order polarization array is first encoded into the spatial-coherence matrix of the source. We demonstrate that the encoded higher-order polarization array can then be reconstructed well in the received plane even when the partially coherent source is significantly blocked by an opaque obstacle or experiences strong phase perturbation. This highlights the high robustness of the synthesized higher-order polarization array. Additionally, we discuss the influence of the spatial-coherence area of the source on the robustness of the beam arrays. The findings of this work may have practical implications for multiparticle manipulation and multichannel optical communication in complex environments.

DOI: 10.1103/PhysRevApplied.20.054031

I. INTRODUCTION

Optical beams with structured profiles in their intensity, phase, and polarization have garnered significant attention over the past several decades [1]. Compared to single-structured beams, beam arrays with structured physical properties offer extended scope for applications and numerous advantages in various fields, including multiparticle manipulation [2], laser cutting and punching [3], and multichannel optical communication [4]. Structured beam arrays are typically generated through fully coherent light-modulation methods, such as those employing spatial light modulators [5], metasurfaces [6], integrated photonics platforms [7], and spin-orbital interactions of light [8]. However, due to the fully coherent modulation, the speckle effect cannot be ignored in the resulting beam arrays [9].

Optical coherence is another fundamental character of light fields, which has played a vital role in understanding the interference, propagation, and light-matter interactions of both classical and quantum wave fields [10]. It has been well recognized that optical beams with reduced spatial coherence, i.e., partially coherent beams, have unique advantages in a variety of applications, including high-quality optical imaging [11–13], optical encryption [14], optical trapping [15,16], and free-space optical communications [17,18]. In the application of optical beam shaping, it has been demonstrated that optical coherence can be viewed as a novel degree of freedom to shape the beam profile into the desired form [19]. In particular, in partially coherent beam shaping, the speckle effect can be greatly suppressed due to the low spatial-coherence property.

Recently, a method based on partially coherent light modulation has been proposed to synthesize high-quality structured beam arrays [20–23]. This approach engineers the second-order spatial-coherence structure of the beam source into a latticelike distribution, enabling the structured amplitude, phase, and polarization from the beam source to be mapped into the beam arrays formed in the far field. However, this technique still faces challenges when perturbations occur in the physical quantities of the beam source, leading to distortions in the resulting beam arrays.

To this end, in this work, we propose an alternative method to synthesize robust beam arrays carrying structured polarization states. The method is based on the vectorial spatial-coherence-structure engineering [24,25] of a partially coherent beam source. The fully coherent structured polarization array is first encoded into the spatial-coherence matrix of the partially coherent vectorial

*yongleiliu2019@163.com
†fwang@suda.edu.cn
‡yangjian_cai@163.com
§yahongchen@suda.edu.cn

source and then recovered during beam propagation. We demonstrate that even when the beam source encounters perturbations, such as opaque obstacles or random phase variations, the structured polarization array can still be accurately reconstructed in the received plane, highlighting its high robustness property.

This work is organized as follows. In Sec. II, we present the beam model for the higher-order polarization array. In Sec. III, we show the principle for vectorial spatial-coherence-structure engineering, in which the higher-order polarization array is encoded into the spatial-coherence matrix of a partially coherent vectorial beam source. Experimental synthesis of the fully coherent and partially coherent higher-order polarization array is discussed in Sec. IV. The effect of the spatial-coherence area and obstacle size on the robustness of the synthesized partially coherent higher-order polarization array, as well as the robustness property of the higher-order polarization array under random phase perturbations, is also studied in the same section. Finally, in Sec. V, we summarize our findings.

II. HIGHER-ORDER POLARIZATION ARRAY

We assume that the beam array carries the structured polarization states that are located on the higher-order Poincaré spheres [26]. Its electric field can be expressed as

$$\mathbf{E}(\mathbf{v}) = \sum_{m=1}^{M} \mathbf{a}(\mathbf{v} - \mathbf{v}_m, \Theta_m, \Phi_m), \tag{1}$$

where $\mathbf{v}$ represents the spatial position vector, M is the total number of higher-order polarization states embedded in the beam, and $\mathbf{a}(\mathbf{v} - \mathbf{v}_m, \Theta_m, \Phi_m)$ denotes the electric field of the mth higher-order polarization state with $\mathbf{v}_m$ being the spatial displacement and $\Theta_m \in [0, \pi]$ and $\Phi_m \in [0, 2\pi)$ being the polar and azimuthal angles in the spherical coordinates of the higher-order Poincaré sphere, respectively. The field of the mth higher-order polarization state can be expressed as a superposition of complex vector amplitudes of the modes at the north and south poles of a higher-order Poincaré sphere, i.e.,

$$\mathbf{a}(\mathbf{v} - \mathbf{v}_m, \Theta_m, \Phi_m) = \cos\left(\frac{\Theta_m}{2}\right) \mathrm{e}^{-\mathrm{i}\frac{\Phi_m}{2}} \mathbf{a}_N(\mathbf{v} - \mathbf{v}_m) + \sin\left(\frac{\Theta_m}{2}\right) \mathrm{e}^{\mathrm{i}\frac{\Phi_m}{2}} \mathbf{a}_S(\mathbf{v} - \mathbf{v}_m), \tag{2}$$

where $\mathbf{a}_N(\mathbf{v} - \mathbf{v}_m) = \mathcal{L}_{p_N, l_N}(\mathbf{v} - \mathbf{v}_m)\hat{\mathbf{e}}_R$ and $\mathbf{a}_S(\mathbf{v} - \mathbf{v}_m) = \mathcal{L}_{p_S, -l_S}(\mathbf{v} - \mathbf{v}_m)\hat{\mathbf{e}}_L$ are the modes at the north and south poles, respectively, with $\mathcal{L}_{p,l}$ being the Laguerre-Gaussian mode with radial index p and azimuthal index l, and $\hat{\mathbf{e}}_R$ and $\hat{\mathbf{e}}_L$ being the unit vectors for the right-handed and left-handed circular-polarization states. The shape of the higher-order polarization array can be controlled by governing the parameters $\mathbf{v}_m$, Θ_m, Φ_m, and M.

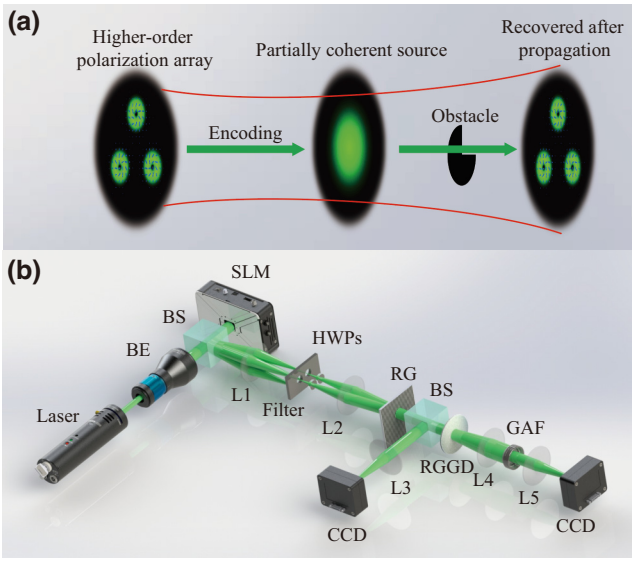

FIG. 1. (a) A schematic for encoding a higher-order polarization array into the vectorial spatial-coherence structure of a partially coherent source and decoding it during beam propagation. The obstacle placed in the transmission link is used to examine the robustness of the recovered higher-order polarization array. (b) The experimental setup for synthesizing and encoding the higher-order polarization array, as well as measuring the robustness of the synthesized higher-order polarization array.

As shown in Eq. (1), the individual polarization states in the electric field are phase locked. Consequently, when such a polarization array is carried by a conventional fully coherent beam, it undergoes distortion during propagation due to multiple interferences among the individual polarization states [see Figs. 2(a)–2(d)]. Even if the phase-locking condition is relaxed, the spatial distribution of each individual polarization state will still experience distortion during propagation in an optical system with disturbances, such as when obstructed by an opaque obstacle [see Figs. 2(e) and 2(f)] or subjected to fluctuating turbulence [see Figs. 5(b) and 5(e)].

III. VECTORIAL SPATIAL-COHERENCE-STRUCTURE ENGINEERING

We now turn to discussing the generation of a robust higher-order polarization state array. In our method, the higher-order polarization state described by Eq. (1) is first encoded into the vectorial spatial-coherence structure of a partially coherent source [see Fig. 1(a)]. The statistical properties of the source are characterized by the

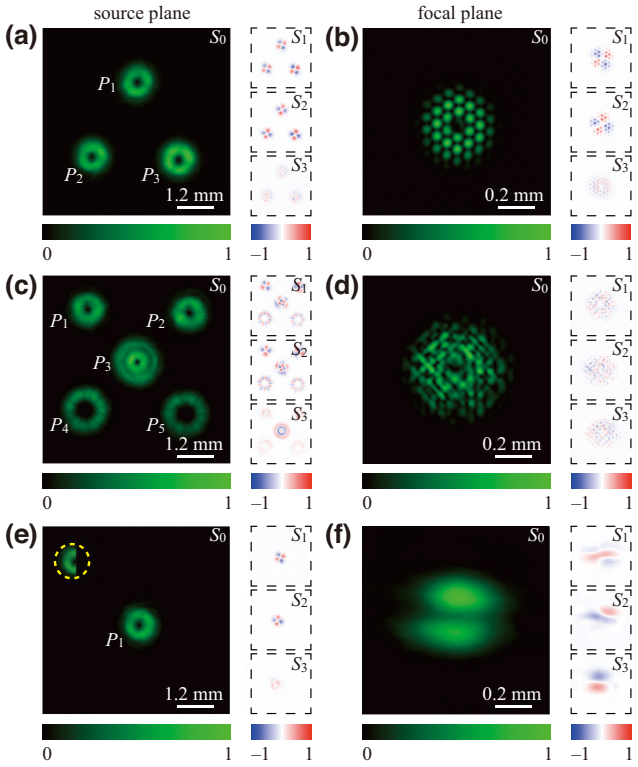

FIG. 2. The experimental results for the measured Stokes parameters S_0, S_1, S_2, and S_3 of the fully coherent higher-order polarization arrays (a),(c),(e) in the source plane and (b),(d),(f) in the focal plane. In (a) and (b), the polarization parameters for all beamlets (P_1, P_2, and P_3) are set as $\Theta = \pi/2$, $\Phi = -\pi/3$, $l_N = l_S = 1$, and $p_N = p_S = 0$. In (c) and (d), the parameters for P_1 are $\Theta = \pi/2$, $\Phi = -\pi/3$, $l_N = l_S = 1$, and $p_N = p_S = 0$; those for P_2 are $\Theta = \pi/2$, $\Phi = -\pi$, $l_N = l_S = 1$, and $p_N = p_S = 0$; those for P_3 are $\Theta = \pi/2$, $\Phi = -\pi/3$, $l_N = l_S = 1$, $p_N = 0$, and $p_S = 1$; those for P_4 are $\Theta = \pi/2$, $\Phi = -\pi/3$, $l_N = l_S = 3$, and $p_N = p_S = 0$; and those for P_5 are $\Theta = \pi/2$, $\Phi = -\pi$, $l_N = l_S = 3$, and $p_N = p_S = 0$. In (e) and (f), the source is blocked by a sector-shaped obstacle with the opening angle π.

cross-spectral density matrix, i.e.,

$$W_{\alpha\beta}(\mathbf{r}_1, \mathbf{r}_2) = T^*_\alpha(\mathbf{r}_1) T_\beta(\mathbf{r}_2) \mu_{\alpha\beta}(\mathbf{r}_1, \mathbf{r}_2), \tag{3}$$

where $W_{\alpha\beta}(\mathbf{r}_1, \mathbf{r}_2)$ with $(\alpha, \beta) = (x, y)$ are the elements of the 2×2 coherence matrix, $\mathbf{r}_1$ and $\mathbf{r}_2$ are two arbitrary transverse spatial position vectors in the cross section of the beam, and $T_x(\mathbf{r})$ and $T_y(\mathbf{r})$ denote the complex amplitudes for the field components along the x and y directions, respectively. $\mu_{\alpha\beta}(\mathbf{r}_1, \mathbf{r}_2)$ are the normalized correlation functions between the field components along the α and β directions at $\mathbf{r}_1$ and $\mathbf{r}_2$ and are modulated by the encoded polarization state via [24,27]

$$\mu_{\alpha\beta}(\mathbf{r}_1, \mathbf{r}_2) = K_{\alpha\beta} \iint \Phi_{\alpha\beta}(\mathbf{v}) \exp[-\mathrm{i}(\mathbf{r}_1 - \mathbf{r}_2) \cdot \mathbf{v}] \mathrm{d}^2\mathbf{v}. \tag{4}$$

Above, $\mathbf{\Phi}(\mathbf{v}) = \mathbf{E}^*(\mathbf{v})\mathbf{E}^{\mathrm{T}}(\mathbf{v})$, with the asterisk and superscript T denoting the complex conjugate and matrix transpose, respectively, are the elements of a 2×2 polarization matrix for the higher-order polarization array and $K_{\alpha\beta}$ are the factors that normalize the correlation functions.

Remarkably, when the encoded polarization states are located on the equators of the higher-order Poincaré spheres and the amplitudes $T_x(\mathbf{r}) = T_y(\mathbf{r})$, the partially coherent source described by Eq. (3) remains completely unpolarized. Nonetheless, the encoded higher-order polarization array will manifest during the beam propagation [see Fig. 1(a)]. The polarization matrix of the beam after propagation through a stigmatic ABCD optical system is obtained as [24]

$$\Phi_{\alpha\beta}(\boldsymbol{\rho}) \propto \left[\tilde{\mathcal{A}}^*_\alpha\left(\frac{\boldsymbol{\rho}}{\lambda B}\right) \tilde{\mathcal{A}}_\beta\left(\frac{\boldsymbol{\rho}}{\lambda B}\right)\right] \otimes \tilde{\mu}_{\alpha\beta}\left(\frac{\boldsymbol{\rho}}{\lambda B}\right), \tag{5}$$

where $\boldsymbol{\rho}$ is the spatial position vector in the output plane, the tilde ("~") denotes the Fourier transform, $\otimes$ signifies the convolution, and $\mathcal{A}_\alpha(\mathbf{r}) = T_\alpha(\mathbf{r}) \exp(\mathrm{i}kA\mathbf{r}^2/2B)$ with $k = 2\pi/\lambda$ being the wave number (λ being the wavelength), and A and B being the elements of the ABCD transform matrix. It is found from the convolution relation of Eq. (5) that when the spatial coherence is low enough, i.e., the Fourier transforms of the spatial correlation functions $\tilde{\mu}_{\alpha\beta}$ are much slower functions of the argument than $\tilde{\mathcal{A}}_\alpha$ and $\tilde{\mathcal{A}}_\beta$, the polarization matrix in the received plane is determined mainly by the spatial-coherence structure of the partially coherent beam source, i.e.,

$$\Phi_{\alpha\beta}(\boldsymbol{\rho}) \propto \tilde{\mu}_{\alpha\beta}\left(\frac{\boldsymbol{\rho}}{\lambda B}\right). \tag{6}$$

Meanwhile, considering Eq. (4), we observe that the Fourier transforms of the spatial correlation functions are directly proportional to the polarization matrix of the encoded higher-order polarization array. Consequently, during the beam propagation, the encoded higher-order polarization array can be accurately reconstructed. Moreover, we discover from Eq. (5) that even when the beam source undergoes perturbations, such as being obstructed by an opaque obstacle with an opening area $S_o \gg S_c$ (where S_c denotes the spatial-coherence area of the source), the encoded higher-order polarization array can still be effectively recovered. This observation highlights the capability of generating a robust higher-order polarization array through the vectorial spatial-coherence engineering of a partially coherent source.

IV. SYNTHESIZING HIGHER-ORDER POLARIZATION ARRAY

We show in Fig. 1(b) the experimental setup for synthesizing and encoding the higher-order polarization array into the vectorial spatial-coherence structure of a partially

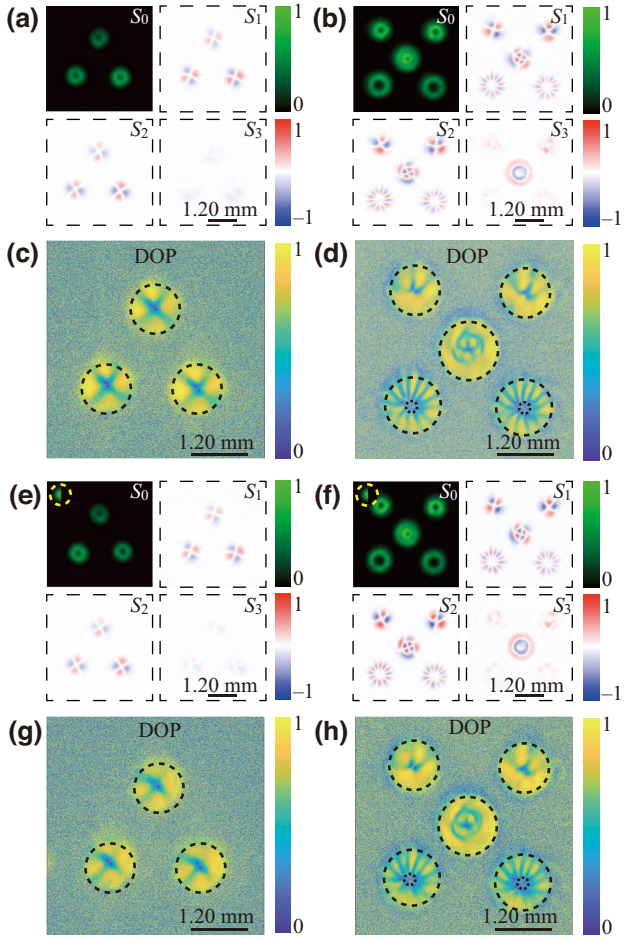

FIG. 3. The experimental results for the focal-plane Stokes parameters and the DOPs of two types of higher-order polarization arrays generated by the partially coherent sources (a)–(d) without an obstacle and (e)–(h) with a sector-shaped obstacle with opening angle π.

coherent beam source, as well as measuring its robustness. As depicted in Fig. 1(b), a linearly polarized beam emitted from a diode-pumped solid state laser (with wavelength $\lambda = 532$ nm) passes through a beam expander (BE) and then goes into a reflective phase-only spatial light modulator (SLM). The SLM is capable of generating various optical modes through the implementation of computer-generated holograms (CGHs). Here, a multiplexed CGH [25] is employed to simultaneously generate two scalar modes, denoted as $E_x(\mathbf{v})$ and $E_y(\mathbf{v})$. These scalar modes represent the amplitudes of the x and y components of the electric field $\mathbf{E}(\mathbf{v})$ in the higher-order polarization array.

The imprinted phase profile on the multiplexed CGH is given by $\Psi(p,q) = \Psi_x(p,q) + \Psi_y(p,q)$, where $\Psi_x(p,q)$ and $\Psi_y(p,q)$ denote the profiles for $E_x(\mathbf{v})$ and $E_y(\mathbf{v})$, respectively, and (p,q) are the pixel coordinates. The profiles are of the form $\Psi_j(p,q) = \mathcal{M}_j(p,q)\text{Mod}[\mathcal{F}_j(p,q) + a_j 2\pi p/\Lambda + 2\pi q/\Lambda, 2\pi]$, where $\mathcal{M}_j(p,q) = 1 + (1/\pi)\text{sinc}^{-1}[A_j(p,q)]$, $\mathcal{F}_j(p,q) = \phi_j(p,q) - \pi\mathcal{M}_j(p,q)$ with $A_j(p,q)$ and $\phi_j(p,q)$ being the amplitude and phase for the complex function $E_j(\mathbf{v})$, $j \in (x,y)$, and Mod denotes the modulo operation. The term $a_j 2\pi p/\Lambda + 2\pi q/\Lambda$ is used to generate a blazed grating pattern, with the parameter Λ controlling its spatial period and $a_x = -a_y = -1$ ensuring that the gratings for $\Psi_x(p,q)$ and $\Psi_y(p,q)$ are at angles of -45° and $+45^\circ$, respectively, to the p axis while the corresponding diffraction orders are in planes oriented orthogonally to the grating lines.

The diffracted light from the SLM goes into a $4f$ common-path interferometric system composed of two thin lenses, L1 and L2, with the SLM being placed in the input plane of the system. In the spatial frequency domain (the rear focal plane of L1), a two-pinhole filter extracts the two $+1$ diffraction orders, with amplitudes corresponding to $E_x(\mathbf{v})$ and $E_y(\mathbf{v})$, respectively. The half-wave plates (HWPs) are then utilized to transform these beams into x- and y-polarized states. In the output plane of the $4f$ system (the rear focal plane of L2), a Ronchi grating (RG) is employed to superpose the two modes [28], resulting in a single vector mode that carries the desired higher-order polarization array.

A. Fully coherent case

The output beam from the RG is fully coherent and is split into two portions by a beam splitter (BS). In the first portion, we examine the focusing properties of the fully coherent beam carrying the higher-order polarization array. In Figs. 2(a) and 2(c), we present the experimental results for the measured Stokes parameters S_0, S_1, S_2, and S_3 of the synthesized fully coherent higher-order polarization arrays at the source plane (after the RG), while Figs. 2(b) and 2(d) show the corresponding experimental results in the focal plane. The polarization parameters for all beamlets are provided in the figure caption. We note here that in our experiment the Stokes parameters for the fully coherent and partially coherent structured beams are measured using the standard method [29] by inserting the linear polarizer, half-wave plate, and quarter-wave plate into the optical path. From the experimental results, we observe that the higher-order polarization arrays are synthesized well in the source plane. However, during free-space propagation, the polarization states become distorted due to multiple instances of interference among the individual beamlets. In Figs. 2(e) and 2(f), we show the measured Stokes parameters for a single higher-order polarization state in the source plane and in the focal plane. In the experiment, the single higher-order polarization state is blocked in the source plane by a sector-shaped obstacle with an opening angle of π. Consequently, the polarization state in the focal plane is distorted, indicating that even when the individual polarization states are uncorrelated (not phase locked),

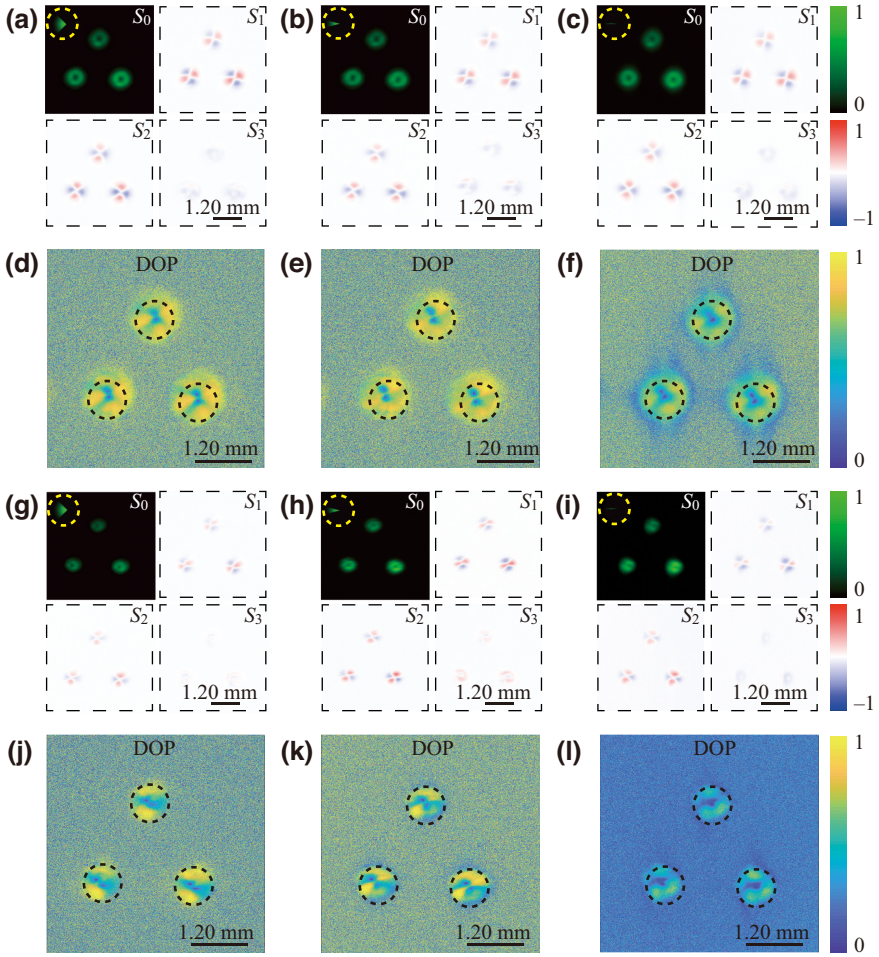

FIG. 4. The experimental results for the focal-plane Stokes parameters and the DOPs of the higher-order polarization arrays generated by the partially coherent sources with initial spatial-coherence width (a)–(f) $\delta_0 = 0.1$ mm and (g)–(l) $\delta_0 = 0.2$ mm. The partially coherent source is blocked by the sector-shaped obstacle with opening angle (a),(d),(g),(j) $\pi/2$, (b),(e),(h),(k) $\pi/6$, and (c),(f),(i),(l) $\pi/36$.

distortion will still occur during the propagation of the beam in an optical system with disturbances.

B. Partially coherent case

In the second portion, the polarization state of the higher-order polarization array is encoded into the vectorial spatial-coherence structure of a partially coherent beam. The synthesized fully coherent beam first passes through a rotating ground-glass disk (RGGD) that renders the beam spatially incoherent. We note that the beam, after passing through the RGGD, remains fully polarized and in the same polarization state as before. In our experiment, the diameter of the beam spot on the RGGD is significantly larger than the inhomogeneity scale of the RGGD, confirming that the beam after the RGGD can be considered spatially incoherent [9]. After the incoherent light beam passing through a thin lens (L4) and a Gaussian amplitude filter (GAF), the cross-spectral density matrix of the output partially coherent beam is obtained by

$$W_{\alpha\beta}(\mathbf{r}_1,\mathbf{r}_2) = \iint W_{\alpha\beta}(\mathbf{v}_1,\mathbf{v}_2) H^*_{\alpha}(\mathbf{r}_1,\mathbf{v}_1) \times H_{\beta}(\mathbf{r}_2,\mathbf{v}_2)\mathrm{d}^2\mathbf{v}_1\mathrm{d}^2\mathbf{v}_2, \quad (7)$$

where $W_{\alpha\beta}(\mathbf{v}_1,\mathbf{v}_2) = \Phi_{\alpha\beta}(\mathbf{v}_1)\delta(\mathbf{v}_1-\mathbf{v}_2)$ is the cross-spectral density matrix for the spatially incoherent beam, with $\Phi_{\alpha\beta}(\mathbf{v}_1)$ being its polarization matrix and $\delta(\mathbf{v}_1-\mathbf{v}_2)$ being the Dirac delta function. $H_x(\mathbf{r},\mathbf{v})$ and $H_y(\mathbf{r},\mathbf{v})$ are the response functions of the optical system between the incoherent and synthesized partially coherent sources, which are expressed as

$$H_x(\mathbf{r},\mathbf{v}) = H_y(\mathbf{r},\mathbf{v}) = T(\mathbf{r})\frac{-\mathrm{i}\exp(\mathrm{i}kf)}{\lambda f}\exp\left[\frac{\mathrm{i}\pi}{\lambda f}(\mathbf{v}^2 - 2\mathbf{r}\cdot\mathbf{v})\right], \quad (8)$$

with $T(\mathbf{r}) = \exp[-\mathbf{r}^2/(2\sigma_0)^2]$ denoting the transmission function of the GAF (σ_0 specifying the width of the beam) and f being the focal distance of the thin lens L4. Taking $W_{\alpha\beta}(\mathbf{v}_1,\mathbf{v}_2)$, $H_x(\mathbf{r},\mathbf{v})$, and $H_y(\mathbf{r},\mathbf{v})$ into Eq. (7), we obtain that the cross-spectral density matrix of the output beam has the same form as Eqs. (3) and (4), indicating that the higher-order polarization array is now encoded into the spatial-coherence structure of the synthesized partially coherent source. In addition, we find that the spatial-coherence width δ_0 of the synthesized source is controlled

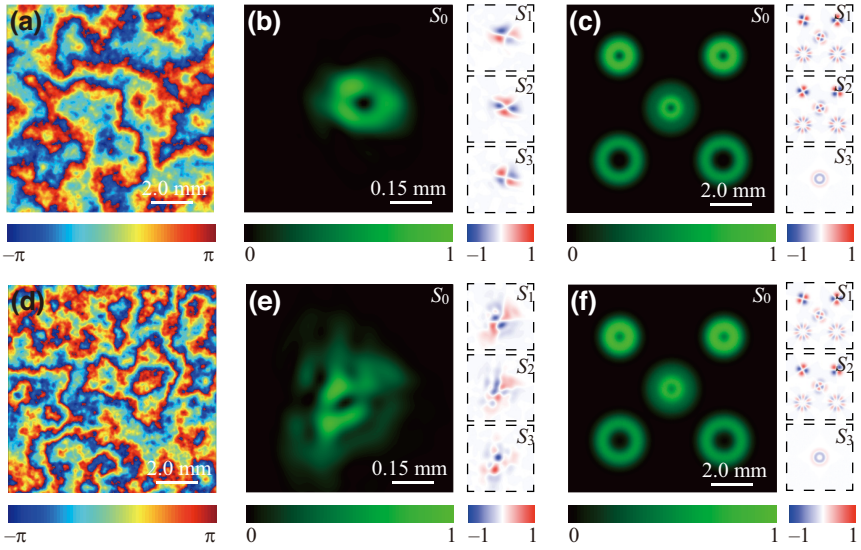

FIG. 5. The simulation results for (a),(d) the spatial distributions of the random phase perturbations, (b),(e) the focal-plane Stokes parameters of the higher-order polarization state generated by the fully coherent source, and (c),(f) the focal-plane Stokes parameters of the higher-order polarization state generated by the partially coherent source under the phase perturbations with (a)–(c) $C_n^2 = 5 \times 10^{-15}$ m$^{-2/3}$ and (d)–(f) $C_n^2 = 1 \times 10^{-14}$ m$^{-2/3}$.

by the beam waist w_0 of the Laguerre-Gaussian mode in Eq. (2), i.e., $\delta_0 = \lambda f/(\pi w_0)$.

To demonstrate the effectiveness of our proposed strategy, we now examine the focusing property of the synthesized partially coherent beam. Figures 3(a)–3(d) display the experimental results for the measured focal-plane Stokes parameters and the degree of polarization (DOP) for the two types of higher-order polarization arrays. We find that the encoded higher-order polarization arrays are accurately recovered in the focal plane and that the resulting beam arrays exhibit a high DOP. It is remarkable that both of the partially coherent sources show a Gaussian intensity distribution and are completely unpolarized. To show the robustness of the higher-order polarization arrays, we present in Figs. 3(e)–3(h) the experimental results of the focal-plane Stokes parameters and the DOPs of the two types of higher-order polarization arrays when their sources are partially blocked by a sector-shaped obstacle with an opening angle of π. It is found that the focal-plane higher-order polarization arrays can still be recovered well, with the spatial distributions of the Stokes parameters and the DOPs being almost unaffected by the obstacle in the source plane.

C. Effect of spatial-coherence area and obstacle size

To investigate the influence of the spatial-coherence area and obstacle size on the robustness of the focal-plane higher-order polarization arrays, we show in Fig. 4 the experimental results of the focal-plane Stokes parameters and the DOPs of the higher-order polarization arrays generated by the partially coherent sources with different initial spatial-coherence widths. The partially coherent sources are obstructed by the sector-shaped obstacles with opening angles of $\pi/2$, $\pi/6$, and $\pi/36$, respectively. We note that, in Fig. 3, the initial spatial-coherence width is $\delta_0 = 0.1$ mm. The initial spatial-coherence width is controlled by adjusting the beam waist of the Laguerre-Gaussian mode, which is used to synthesize the fully coherent higher-order polarization array. As we decrease the beam waist, the initial spatial width increases.

We find from Figs. 4(a)–4(c) that when $\delta_0 = 0.1$ mm, the focal-plane higher-order polarization array can be reconstructed well for the obstacles with three different opening angles. Nevertheless, it is found from Figs. 4(d)–4(f) that with the decrease of the opening angle, the DOP of the beam array decreases slightly. Even for the smallest opening angle of $\pi/36$, we find in the significant intensity region (inside the dashed circle) that the field is still highly polarized [see Fig. 4(d)]. We now increase the initial spatial-coherence width to $\delta_0 = 0.2$ mm and observe distortions appearing in the spatial distributions of the Stokes parameters when the beam source is blocked. This is because when the opening area of the obstacle is comparable to, or smaller than, the spatial-coherence area of the source, the focal-plane polarization state is determined by both the initial amplitude (affected by the obstacle) and the spatial-coherence structure of the beam [see Eq. (5)]. As the opening area decreases, we observe an increase in the distortions of the Stokes parameters and a decrease in the DOP. Comparing the DOP for $\delta_0 = 0.2$ mm [Fig. 4(l)] with the DOP for $\delta_0 = 0.1$ mm [Fig. 4(f)] under the condition when the opening angle of the obstacle is $\pi/36$, we find a significant decrease in the DOP, with an increase in δ_0. These observations suggest that the robustness of the focal-plane higher-order polarization array can be enhanced by reducing the spatial coherence of the partially coherent source.

D. Robustness of higher-order polarization array under phase perturbation

Finally, we examine the robustness of the focal-plane higher-order polarization array under the condition when

the beam source experiences phase perturbation. Two types of phase perturbations are generated, based on the Kolmogorov turbulence-statistics theory and the Rytov perturbation approximation [30,31], as depicted in Figs. 5(a) and 5(d), respectively. The corresponding generalized refractive-index structure parameters are set to $C_n^2 = 5 \times 10^{-15}$ $m^{-2/3}$ and 1×10^{-14} $m^{-2/3}$ for Figs. 5(a) and 5(d), representing scenarios of medium strong and strong turbulence, respectively. In Figs. 5(b) and 5(e), we present simulation results for the focal-plane Stokes parameters of a focused fully coherent beam carrying a single higher-order polarization state under the two different phase perturbations. As the perturbation strength increases, we observe distortion in both the intensity and the polarization state of the fully coherent beam. However, in contrast, Figs. 5(c) and 5(f) display the focal-plane Stokes parameters of a focused partially coherent beam subjected to the same phase perturbations. Remarkably, we find that even under both medium strong and strong phase perturbations, the higher-order polarization array remains well recovered. The random phase perturbations discussed here are synthesized typically by the SLM, which, however, only responds to the linearly polarized light. In our case, the beam shows vectorial polarization states. As a result, the SLM cannot be used in our experiment for realizing the random phase perturbations. The specially customized phase plates may be the possible solution for creating the random phase perturbations for our case.

V. CONCLUSIONS

In summary, we have introduced a protocol for synthesizing beam arrays with controllable higher-order polarization states in their individual beamlets. This method utilizes vectorial spatial-coherence engineering, wherein the higher-order polarization arrays are encoded in the spatial-coherence matrix of a partially coherent source. We have demonstrated that the beam arrays carrying higher-order polarization states and exhibiting a high degree of polarization can be recovered well in the focal plane even through their partially coherent beam sources are completely unpolarized and show only a single Gaussian spot. In addition, by measuring the focal-plane Stokes parameters under the condition when the beam source is partially blocked by an opaque obstacle or disturbed by the random phase perturbation, we have found that the higher-order polarization arrays generated in the focal plane are highly robust against the perturbations provided that the spatial-coherence width of the source is sufficiently small. Our results provide a simple and flexible way to generate beam arrays with complex polarization states in a harsh environment and may find applications in information encoding and transmission through complex media.

ACKNOWLEDGMENTS

This work was supported by the National Key Research and Development Program of China (Grants No. 2022YFA1404800 and No. 2019YFA0705000), the National Natural Science Foundation of China (Grants No. 11974218, No. 12192254, No. 12274310, and No. 92250304), and the Jiangsu Funding Program for Excellent Postdoctoral Talent (Grant No. 2023ZB185).

[1] A. Forbes, M. de Oliveira, and M. R. Dennis, Structured light, Nat. Photonics **15**, 253 (2021).
[2] Y. Yang, Y. Ren, M. Chen, Y. Arita, and C. Rosales-Guzmán, Optical trapping with structured light: A review, Adv. Photonics **3**, 034001 (2021).
[3] M. Meier, V. Romano, and T. Feurer, Material processing with pulsed radially and azimuthally polarized laser radiation, Appl. Phys. A **86**, 329 (2007).
[4] A. E. Willner, H. Huang, Y. Yan, Y. Ren, N. Ahmed, G. Xie, C. Bao, L. Li, Y. Cao, Z. Zhao, J. Wang, M. P. J. Lavery, M. Tur, S. Ramachandran, A. F. Molisch, N. Ashrafi, and S. Ashrafi, Optical communications using orbital angular momentum beams, Adv. Opt. Photonics **7**, 66 (2015).
[5] L. Guo, Z. Feng, Y. Fu, and C. Min, Generation of vector beams array with a single spatial light modulator, Opt. Commun. **490**, 126915 (2021).
[6] M. Piccardo, M. de Oliveira, A. Toma, V. Aglieri, A. Forbes, and A. Ambrosio, Vortex laser arrays with topological charge control and self-healing of defects, Nat. Photonics **16**, 359 (2022).
[7] X. Qiao, B. Midya, Z. Gao, Z. Zhang, H. Zhao, T. Wu, J. Yim, R. Agarwal, N. M. Litchinitser, and L. Feng, Higher-dimensional supersymmetric microlaser arrays, Science **372**, 403 (2021).
[8] D. Sarenac, D. G. Cory, J. Nsofini, I. Hincks, P. Miguel, M. Arif, C. W. Clark, M. G. Huber, and D. A. Pushin, Generation of a lattice of spin-orbit beams via coherent averaging, Phys. Rev. Lett. **121**, 183602 (2018).
[9] J. W. Goodman, *Speckle Phenomena in Optics* (Roberts and Company Publishers, Greenwood Village, 2006).
[10] L. Mandel and E. Wolf, *Optical Coherence and Quantum Optics* (Cambridge University, Cambridge, United Kingdom, 1995).
[11] Y. Cai and S.-Y. Zhu, Ghost imaging with incoherent and partially coherent light radiation, Phys. Rev. E **71**, 056607 (2005).
[12] B. Redding, M. A. Choma, and H. Cao, Speckle-free laser imaging using random laser illumination, Nat. Photonics **6**, 355 (2012).
[13] Y. Shen, H. Sun, D. Peng, Y. Chen, Q. Cai, D. Wu, F. Wang, Y. Cai, and S. A. Ponomarenko, Optical image reconstruction in 4*f* imaging system: Role of spatial coherence structure engineering, Appl. Phys. Lett. **118**, 181102 (2021).
[14] D. Peng, Z. Huang, Y. Liu, Y. Chen, F. Wang, S. A. Ponomarenko, and Y. Cai, Optical coherence encryption with structured random light, PhotoniX **2**, 6 (2021).

[15] J. M. Auñón and M. Nieto-Vesperinas, Optical forces on small particles from partially coherent light, J. Opt. Soc. Am. A **29**, 1389 (2012).
[16] J. Yu, Y. Xu, S. Lin, X. Zhu, G. Gbur, and Y. Cai, Longitudinal optical trapping and manipulating Rayleigh particles by spatial nonuniform coherence engineering, Phys. Rev. A **106**, 033511 (2022).
[17] J. C. Ricklin and F. M. Davidson, Atmospheric turbulence effects on a partially coherent Gaussian beam: Implications for free-space laser communication, J. Opt. Soc. Am. A **19**, 1794 (2002).
[18] Y. Liu, X. Zhang, Z. Dong, D. Peng, Y. Chen, F. Wang, and Y. Cai, Robust far-field optical image transmission with structured random light beams, Phys. Rev. Appl. **17**, 024043 (2022).
[19] Y. Chen, F. Wang, and Y. Cai, Partially coherent light beam shaping via complex spatial coherence structure engineering, Adv. Phys. X **7**, 2009742 (2022).
[20] S. Zhu, J. Wang, X. Liu, Y. Cai, and Z. Li, Generation of arbitrary radially polarized array beams by manipulating correlation structure, Appl. Phys. Lett. **109**, 161904 (2016).
[21] C. Liang, X. Zhu, C. Mi, X. Peng, F. Wang, Y. Cai, and S. A. Ponomarenko, High-quality partially coherent Bessel beam array generation, Opt. Lett. **43**, 3188 (2018).
[22] Y. Liu, Z. Dong, F. Wang, Y. Chen, and Y. Cai, Generation of a higher-order Poincaré sphere beam array with spatial coherence engineering, Opt. Lett. **47**, 5220 (2022).
[23] Y. Liu, Z. Dong, F. Wang, Y. Cai, and Y. Chen, Experimental synthesis of higher-order Poincaré sphere beam array with spatial coherence engineering, Appl. Phys. Lett. **122**, 161106 (2023).
[24] Z. Dong, Y. Chen, F. Wang, Y. Cai, A. T. Friberg, and T. Setälä, Encoding higher-order polarization states into robust partially coherent optical beams, Phys. Rev. Appl. **18**, 034036 (2022).
[25] Z. Dong, Y. Zhu, Y. Liu, F. Wang, Y. Cai, T. Setälä, and Y. Chen, Compact generation of light beams carrying robust higher-order Poincaré polarization states, Appl. Phys. Lett. **122**, 221101 (2023).
[26] G. Milione, H. I. Sztul, D. A. Nolan, and R. R. Alfano, Higher-order Poincaré sphere, Stokes parameters, and the angular momentum of light, Phys. Rev. Lett. **107**, 53601 (2011).
[27] F. Gori, V. Ramírez-Sánchez, M. Santarsiero, and T. Shirai, On genuine cross-spectral density matrices, J. Opt. A: Pure Appl. Opt. **11**, 085706 (2009).
[28] X.-L. Wang, J. Ding, W.-J. Ni, C.-S. Guo, and H.-T. Wang, Generation of arbitrary vector beams with a spatial light modulator and a common path interferometric arrangement, Opt. Lett. **32**, 3549 (2007).
[29] P. Meemon, M. Salem, K.-S. Lee, M. Chopra, and J. P. Rolland, Determination of the coherency matrix of a broadband stochastic electromagnetic light beam, J. Mod. Opt. **55**, 2765 (2008).
[30] L. C. Andrews and R. L. Phillips, *Laser Beam Propagation through Random Media* (SPIE Press, Bellinghan, 2005), 2nd ed.
[31] J. M. Martin and S. M. Flatté, Intensity images and statistics from numerical simulation of wave propagation in 3-D random media, Appl. Opt. **27**, 2111 (1988).